RESEARCH PAPER

Resistance of Alkali-activated Slag Cement Against Sodium Sulfate

A. Allahverdi[1,2*], H. Hashemi[1], M. Mahinroosta[1]

** ali.allahverdi@iust.ac.ir*

Received: January 2019 **Revised: June 2019** **Accepted: December 2019**

[1] Research laboratory of Inorganic Chemical Process Technologies, School of Chemical Engineering, Iran University of Science and Technology, Tehran, Iran.

[2] Cement Research Center, Iran University of Science and Technology, Tehran, Iran.

DOI: 10.22068/ijmse.17.1.23

Abstract: *This work evaluates the resistance of alkali-activated slag (AAS) mortar against sodium sulfate attack. The effects of immersion in 5% sodium sulfate solution under room temperature and wetting-drying cycles on the compressive strength of mortar specimens were considered to evaluate the extent of degradation. Mortar specimens prepared from type II and V Portland cements (PC2 and PC5) in accordance with ASTM standard were also used as a reference. To characterize the chemical products of the degradation process due to sodium sulfate attack, the specimens were also studied by X-ray diffractometry, scanning electron microscopy, and the elemental analysis by energy-dispersive X-ray spectroscopy. After 360 days of exposure to the sodium sulfate solution, PC2, PC5 and AAS cements showed 71, 52 and 45% reduction in compressive strength, respectively. According to the obtained results, AAS cement exhibits a higher sulfate resistance compared to PC2 and PC5.*

Keywords: *Sulfate resistance, Compressive strength, Slag, Alkali-activation.*

1. INTRODUCTION

Alkali-activated slag (AAS) cements are generated by the blending of slags with alkaline solutions. Utilization of blast-furnace slag (BFS) in the manufacture of AAS-based concrete would contribute not only to the development of green technology but also to the development of high-performance concrete-based products. AAS production can also pose the considerable potential to reduce greenhouse gas emissions compared to the Portland cement (PC) process generating almost 1 ton of carbon dioxide for each tone of PC. A comparative study recently conducted on assessment of environmental life cycle revealed that AAS-based concretes and mortars result in about 73% less emission of greenhouse gases, 43% less energy requirement, and about 22-94% reduction in several parameters related to the toxic environmental effects in comparison with those of portland cement-based concretes and mortars [1, 2]. One of the main characteristics of AAS binder is its superior durability performance in aggressive environments as compared to PC [3-5]. Sulfate attack is one of several mechanisms of concrete deterioration which causes significant degradation in concrete structures. Much attention was therefore drawn to provide adequate protection techniques for concrete structures in contact with relatively high sulfate-content surroundings [6-9]. When Portland cement-based concrete is in contact with a source of sulfate ions such as soil, groundwater, and decaying organic materials, reactions between alumina containing compounds and calcium hydroxide (Portlandite) as cement constituents and hydration products and diffusing sulfate ions produce gypsum and ettringite [10-13] as shown in the following reactions [9, 14]:

C_3S (triclacium silicate) + 3H (water) ⇛ CSH (calcium silicate hydrate) + 2CH (Portlandite) (1)

CH (Portlandite) + NS (sodium sulfate) + 2H (water)→CSH_2 (gypsum) + NH (sodium hydroxide) (2)

C_3A (tricalcium aluminate) + $3CSH_2$ (gypsum) + 26H (water)→$C_6AS_3H_{32}$ (ettringite) (3)

C_4ASH_{12} (monosulfate) + $2CSH_2$ (gypsum) + 16H (water)→$C_6AS_3H_{32}$ (ettringite) (4)

[Downloaded from sso.iust.ac.ir on 2025-12-10]

[DOI: 10.22068/ijmse.17.1.23]

Gypsum leads to a net expansion of 224% for the solid particles [15]. Ettringite is expansive in nature, having a lower density compared to other hydration products. Thus, the formation of these products causes expansion, cracking, softening with loss of strength and finally degradation of concrete [9-13]. Utilization of type II (C_3A<8%) and type V (C_3A<5%) PC, in accordance with ASTM standards, as sulfate-resisting cements was established first in the 1930s [16]. Later studies confirmed the positive effects of suitable supplementary cementing materials used in blended cements [17-20] and the superior performance of some non-portland cements in this area [21-23]. A few studies done on sulfate resistance of AAS binder have claimed a different mode of degradation which could provide a superior durability performance in sulfate environment depending on the chemical composition of the slag and its reactivity [4, 24]. Therefore, there is also a research vacuum in this field that needs further experimental work.

The main focus of the present work reported herein is on the development of an AAS cement formulated with blast furnace slag, portland cement and a compound alkali activator. This work emphasizes on the sodium sulfate resistance of the resultant AAS cement by investigating the compressive strength and the length change and employing complementary techniques for better interpretation of results. For this purpose, the compressive strength of mortar specimens was measured and compared to evaluate the extent of degradation. Deteriorated paste specimens were also studied by X-ray diffractometry (XRD), scanning electron microscopy (SEM), and the elemental analysis by energy-dispersive X-ray spectroscopy (EDAX) to characterize the chemical products of sodium sulfate attack.

2. EXPERIMENTAL PROCEDURE

2.1. Materials

BFS was prepared from the Isfahan steel complex in Iran. It was ground to a residue of 1.5 wt% on 90 μm sieve using a laboratory one-cylindrical compartment ball mill (30 cm in length and 26 cm in diameter) containing spherical steel balls. The prepared slag was also characterized for its chemical and mineralogical compositions by wet analysis and XRD. The chemical composition and properties of type II and V portland cements (PC2 & PC5) and BFS determined in accordance with ASTM standards are shown in table 1.

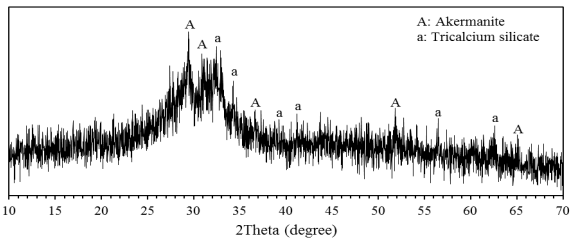

Fig. 1. X-ray diffraction pattern of BFS.

Fig. 1 shows the XRD pattern of BFS. As can be seen, the BFS is mainly amorphous and consists of few amounts of crystalline phases including akermanite ($Ca_2MgO_7Si_2$) and tricalcium silicate (Ca_3SiO_5). These phases were identified based on ICDD standard cards of 01-083-1815 and 01-086-0402, respectively. The tricalcium silicate originates from the reaction between CaO and SiO_2 existed in the melt during the high temperature production process of the BFS.

Table 1. Properties of Portland cements and slag

Oxide (wt.%)	[a]PC2	[b]PC5	BFS
SiO_2	20.26	22.42	36.06
Al_2O_3	5.43	3.81	9.16
Fe_2O_3	3.87	4.20	0.70
CaO	64.96	64.90	36.91
MgO	0.48	0.08	10.21
SO_3	2.09	1.46	1.15
K_2O	0.60	0.42	0.70
Na_2O	0.27	0.22	0.48
TiO_2	-		3.50
MnO	-		1.46
V_2O_5	-		0.10
Free CaO	0.48	1.07	-
LOI	1.95	1.61	-
Bogue's potential phase composition (wt%)			
C_3S	60.51	53.65	
C_2S	12.51	23.88	
C_3A	7.84	2.99	
C_4AF	11.78	12.78	
Fineness (m^2/kg)	320	295	320

[a]Prepared from Dorood cement factory, Iran.
[b]Prepared from Tehran cement factory, Iran.

[Downloaded from sso.iust.ac.ir on 2025-12-10]

[DOI: 10.22068/ijmse.17.1.23]

2.2. Methods

2.2.1. Preparation of Specimens

AAS mortar and paste specimens were prepared using sodium silicate (sodium oxide = 34.04 wt%, silicon dioxide = 31.36 wt%, water = 34.60 wt%) and sodium hydroxide (Merck, purity> 98%) as the constituents of the activator. Standard sand (DIN-EN 196-1) was used to prepare mortar specimens. The workability of fresh AAS mortar was measured using a standard flow table according to the ASTM C1437 and C230. The water-to-slag (w/s) ratio of the AAS mortar was adjusted at 0.43 to achieve a flow between 105 to 115% in 25 drops of the flow table. Sodium silicate, sodium hydroxide, and water were blended at given proportions to produce an alkali-activator with a silica modulus (M_s= mass ratio of silicon dioxide to sodium oxide) equal to 0.40, containing 2.70% sodium oxide by weight of BFS. The sand-to-slag ratio was fixed at 2.75 to enable direct comparison with PC and to obtain reasonable mortar workability. For AAS paste specimens, the w/s ratio, M_s and weight fraction of sodium oxide were adjusted at 0.26, 0.40 and 2.00, respectively. The water-to-cement ratio for Portland cement mortar and paste specimens were fixed at 0.485 and 0.27, respectively. Specimens of Portland cements were prepared in accordance with the ASTM C109 standard. To prepare AAS mortar specimens, the prepared activator was first added to the slag and mixed for 3 min and then sand was added, followed by remixing for 2 more minutes in a planetary mixer. Mortar specimens were cast in 50 mm cubes and 25×25×285 mm^3 prisms for measurements of compressive strength and length change, respectively. Cubic paste specimens of the size 2×2×2 cm^3 were also prepared for XRD and SEM/EDAX studies. All the molds were held at an ambient of more than 95% relative humidity to prevent drying and giving enough time (24 h) to the pastes and mortars to set and harden at laboratory ambient temperature (25±2 °C). After demolding, all the specimens were cured in tap-water kept at 25±2 °C until the testing time.

2.2.2. Compressive Strength Reduction Test

After 28 days of curing, some of the mortar specimens were used for compressive strength measurement. The AAS, PC2, and PC5 mortar specimens exhibited 28-day compressive strength of 52, 63 and 58 MPa, respectively. All the paste and mortar specimens were then used for immersion tests. ASTM C1012 standard was used as the basis for the sulfate resistance test. The cured specimens were immersed in a 5% sodium sulfate solution as the aggressive environment. The temperature of the solution was fixed at 25 °C. 12-hour cycles of wetting and drying were also applied to accelerate the rate of deterioration. To control the pH of the solution between 6 and 8, the solution was renewed every week during the first 2 months, and then once after 3, 4, 5, 6, 8 and 10 months of exposure. The extent of deterioration was evaluated over 12-month exposure time. At predetermined intervals, the specimens were tested to measure the compressive strength reduction. A total of three cubes were used for each measurement. The compressive strength of the specimens exposed to sodium sulfate solution was measured by using a uniaxial digital hydraulic press (SCL STD 30) of 300 kN-capacity with ±1% accuracy and a loading rate of 0.4 MPa/s. The compressive strength reduction was calculated as follows:

$$\text{Compressive strength reduction (\%)} = [(B-A)/A]\times 100 \quad (5)$$

where *A* (in MPa) is the average compressive strength of three specimens after 28 days of curing and *B* (in MPa) is the average compressive strength of three specimens exposed to sulfate solution. The extent of deterioration was also followed by visual observations.

2.2.3. Length Change Test

Length change test was accomplished according to the ASTM standard C1012 using a comparator device with a precision of 0.01 mm. In conformity with this standard, length changes were computed by the following equation [25]:

$$\Delta L = [(L_x - L_i)/L_g]\times 100 \quad (6)$$

[Downloaded from sso.iust.ac.ir on 2025-12-10]

[DOI: 10.22068/ijmse.17.1.23]

in which ΔL (%) is the change in length at the age of x; L_x is the average comparator reading of three bars at the age of x; L_i is the average initial comparator reading of the same three bars, and L_g is nominal gage length. Measurements of length change were done after 1, 2, 3, 4, 8, 13, and 15 weeks and 4, 5, 6, 7, 8, 10, and 12 months exposing to sodium sulfate solution.

2.2.4. X-ray Diffractometry Studies

X-ray diffraction was employed to identify the degradation products. To perform XRD analysis, samples were prepared from deteriorated paste specimens and then finely ground. XRD analyses were made using Siemens D500 using Cu–Kα radiation at 35 kV and 20 mA. The XRD patterns were attained in 2θ range of 5° to 70° by a scanning rate of 1° per minute.

2.2.5. Microstructural Studies

After 360 days of exposure, samples were prepared for SEM studies. Preparation of samples for SEM analysis involved drying at 50 ˚C, cutting to appropriate pieces, and then coating with a gold layer to make conductive samples. SEM analysis in both secondary electron (SE) and back-scattered electron (BSE) modes were made using TESCAN VEGA II (Germany) scanning electron microscope device at an accelerating voltage of 20 kV.

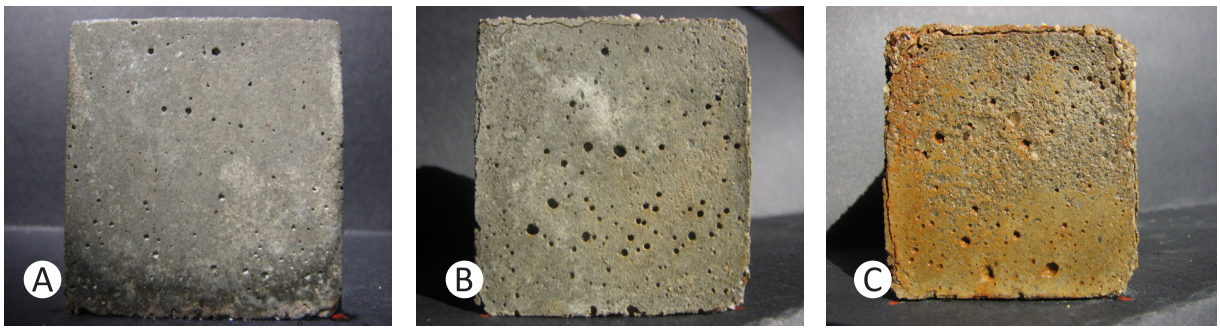

Fig. 2. PC2 mortar specimens exposed to sodium sulfate solution after A: 70 days, B: 140 days, and C: 280 days.

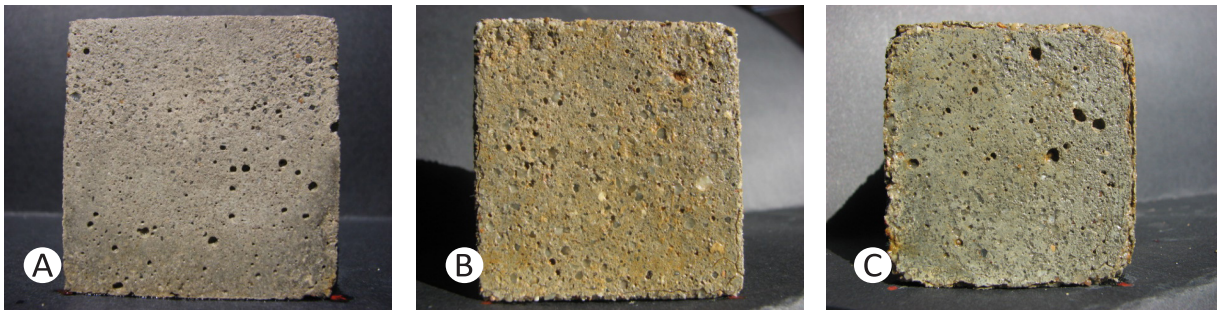

Fig. 3. PC5 mortar specimens exposed to sodium sulfate solution after A: 70 days, B: 140 days, and C: 280 days.

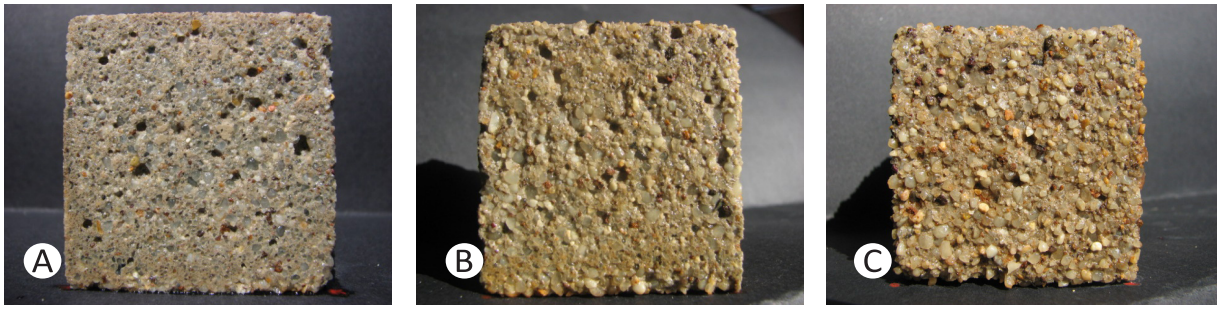

Fig. 4. AAS mortar specimens exposed to sodium sulfate solution after A: 70 days, B: 140 days, and C: 280 days.

[Downloaded from sso.iust.ac.ir on 2025-12-10]

[DOI: 10.22068/ijmse.17.1.23]

3. RESULTS AND DISCUSSION

3.1. Visual Observations

Sulfate attack on portland cement usually results in expansion due to the formation of voluminous products. According to the literature, this expansion gradually manifests itself by cracking at the edges and especially corners of the specimens. Continued expansion can finally lead to the scaling of small pieces at the edges and corners. For the case of AAS specimens, unlike Portland cement no observation has been reported by the researchers. During the course of deterioration, the changes in the appearance of the specimens were monitored visually and photographed. Figs. 2, 3, and 4 show photos prepared from PC2, PC5, and AAS mortar specimens after 70, 140, and 280 days of exposure, respectively. After 70 days of exposure to a sodium sulfate solution, specimens of PC2 and PC5 showed no sign of deterioration. The AAS specimens, however, showed few surface scaling. This surface scaling can be simply recognized by the appearance of the embedded sand particles on the surfaces of the mortar specimens. Prolonged exposure time resulted in the visual appearance of deterioration. As seen in the photos, after 140 days of exposure, specimens of PC5 and especially PC2 showed observable signs of expansion and cracking at the corners and regions close to the edges.

In the case of AAS, continued scaling has changed the appearance of the specimens from cubes of almost smooth surfaces to those of well recognizable coarse surfaces. Accurate inspection of the edges of the specimen in the corresponding photo (Fig. 4) clearly shows the extent of deterioration due to surface scaling. No change in color was recognized except the light brown stains on some surfaces caused by the corrosion of steel net used for suspending specimens in the solution. The steel wires of the net were covered with plastic cover, but the diffusion of the sulfate solution beneath the cover resulted in partial corrosion of the steel wires.

The deterioration signs were more intensified after 280 days of exposure. PC2 and PC5 specimens showed clearly visible signs of deterioration in the form of cracks and scaling at the corners and regions close to the edges. In the case of AAS, the deterioration appeared in the form of more coarsening of the surfaces due to some surface scaling. No visual sign of expansion, e.g. cracking, was observed. Surface scaling in the case of AAS mortar specimens due to sodium sulfate attack has not been reported in the literature. Not only the nature and the properties of the material especially the chemical bonding of the AAS paste to the aggregate but also the mechanism of the sulfate attack and very probably the effects brought about by the relatively high concentration of the sulfate along with the application of wetting-drying cycles are responsible for the scaling phenomenon. According to a recent study [26], this phenomenon seems to be directly related to the ability of the ions (i.e., Na^+) accompanying SO_4^{2-} to alter the pH of the pore solution near the surface in the specimens. The relatively high concentration of the sulfate solution and the application of wetting-drying cycles caused all the specimens undergoing efflorescence in the drying stage. Visual inspections have shown more efflorescence at the corners and regions close to the edges where scaling and coarsening seemed to be more intensified. The growth of sodium sulfate crystals at regions close to the surfaces and especially corners can result in disintegrating stresses. The separation of the AAS paste particles from the aggregates on the surfaces of the mortar specimens is probably due to the crystallization pressure.

3.2. Compressive Strength

The compressive strength changes of different mortar specimens exposed to a sodium sulfate solution at 25 ºC and subjected to wetting-drying cycles are shown in Fig. 5.

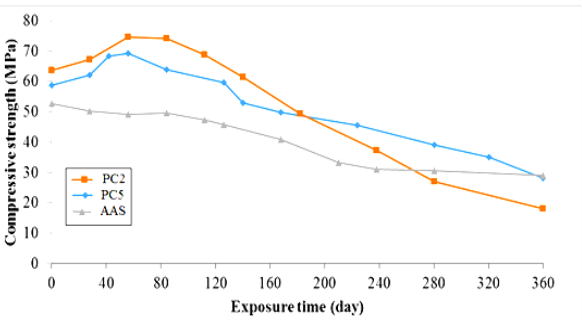

Fig. 5. Compressive strength of specimens subjected to sodium sulfate solution.

[Downloaded from sso.iust.ac.ir on 2025-12-10]

[DOI: 10.22068/ijmse.17.1.23]

As seen, PC2 and PC5 specimens exhibited some increase in compressive strength until 60 days of exposure. This limited increase is due to the progress of hydration reactions inside the specimens and probably to a lesser extent to the deposition of gypsum at regions close to the exposed surfaces resulting in densification. Prolonged exposure, however, resulted in continuous strength reduction. This continuous strength reduction is believed to be due to internal disintegrating stresses exerted by the formation of voluminous compounds including gypsum and ettringite [10, 13].

AAS specimens showed a continuous strength reduction from the beginning of the exposure time with no strength increase. This pattern of strength change confirms the effective termination of the hardening reactions after 28 days of curing and the deteriorating effects of the sodium sulfate attack from the beginning of the exposure time. Such a different behavior compared to portland cements shows the higher vulnerability of AAS specimens during the first several months of exposure. The results obtained from continued exposure, however, showed a different situation. Accurate inspection of the strength changes after 80 days of exposure reveals significantly different strength reduction trends. The steepness of the strength reduction curves considerably decreases in the order of PC2, PC5, and AAS, so that the residual compressive strengths after prolonged exposure time (280 days later) show a different order of sulfate resistance.

To clarify the resulting conclusions, the measured compressive strengths at different time intervals were compared with the corresponding initial values (28-day compressive strengths) and the percentage of the strength reductions were calculated and presented graphically in Fig. 6.

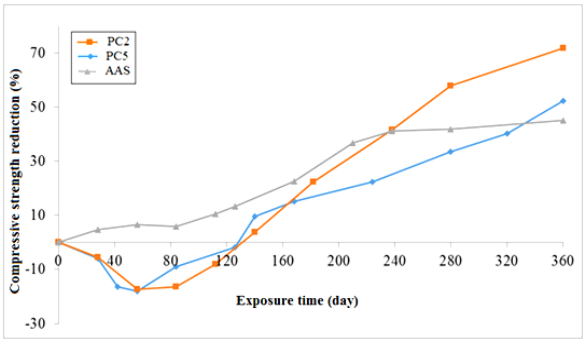

Fig. 6. Compressive strength reduction of specimens subjected to sodium sulfate solution.

The strength reductions after 360 days of exposure for AAS, PC5, and PC2 are 45%, 52% and 71%, respectively. All the three tested cements are more or less vulnerable to sodium sulfate attack. The strength reductions of PC2 and PC5, however, are almost 1.6 and 1.2 times higher than that of AAS, respectively. AAS mortar specimens therefore exhibit a better resistance against sodium sulfate over prolonged exposure time. This result will also be confirmed by further studies in following sections.

3.3. Length Change

The length changes of PC2, PC5, and AAS mortar bars in terms of exposure time to sodium sulfate solution are presented in Fig. 7.

As can be observed in this figure, after about 80 days of exposure to sodium sulfate solution, PC2, PC5, and AAS specimens attained almost the same slight length changes. With continued exposure, the length changes of AAS specimens found a tremendous difference with PC2 and PC5 specimens, so that after 360 days of exposure the PC2, PC5, and AAS mortar bars exhibited 0.36%, 0.24%, and 0.03% length changes, respectively.

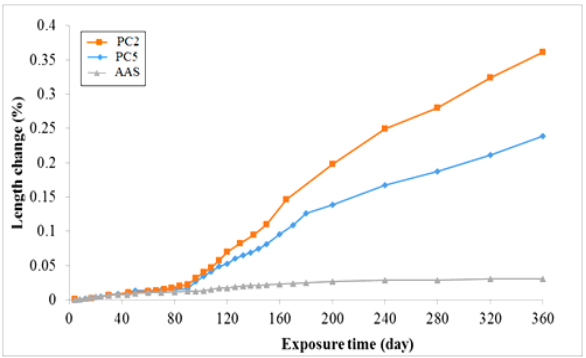

Fig. 7. Length change of PC2, PC5, and AAS mortar bars versus exposure time to sodium sulfate solution.

The obtained results show that AAS mortar bars attained a negligible amount of length change compared to PC2 and PC5 mortar bars. The expansion in PC2 and PC5 is due to the formation of voluminous destructive products such as gypsum and ettringite. In the case of AAS mortar, since BFS does not contain C_3A phase, the probability of the formation of ettringite as

[Downloaded from sso.iust.ac.ir on 2025-12-10]

[DOI: 10.22068/ijmse.17.1.23]

an expansive product is weak. However, AAS showed a trifling expansion during exposure. This can be due to the deposition of sodium sulfate and the growth of its crystals in surface areas. These observations will be discussed later by complementary studies using XRD and SEM/EDAX.

3.4. XRD Studies

The XRD pattern of the 28-day hardened paste of AAS is shown in Fig. 8. As seen, the only crystalline phase in the material is akermanite which was originally present in the starting slag. The other originally present phase, i.e. tricalcium silicate, was consumed in the alkali-activation reactions.

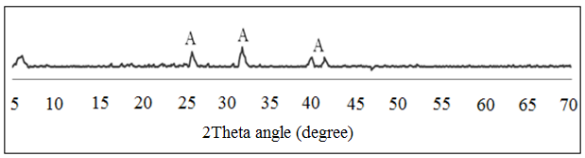

Fig. 8. XRD pattern of 28-day hardened paste of activated slag, A=Akermanite.

Samples were also prepared and analyzed from exposed paste specimens to characterize the chemical products of the degradation process. The obtained diffraction patterns are presented in Fig. 9. As seen, no gypsum and ettringite are present in the AAS sample, whereas considerable amounts of ettringite and gypsum were found in PC samples.

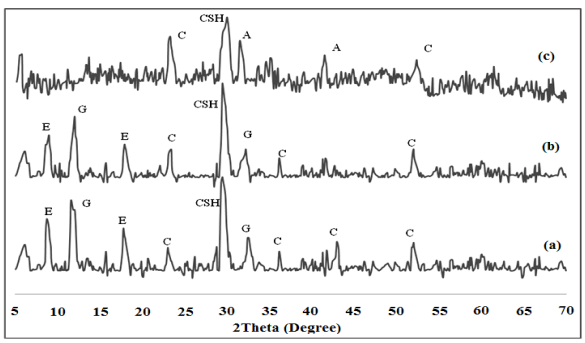

Fig. 9. XRD patterns of paste specimens exposed to 5% sodium sulfate solution: (a) PC2, (b) PC5, and (c) AAS. (E=Ettringite, G=Gypsum, C=Calcite, CSH= calcium silicate hydrate, A=Akermanite).

Upon sulfate attack, the calcium hydroxide present in Portland cement paste directly combines with sulfate ions leading to the formation of gypsum. The alumina-containing hydrates of the Portland cement paste are also converted to ettringite. Formation of these voluminous compounds leads to expansion, cracking, and loss of compressive strength [8, 13, 16]. For the PC pastes, the obtained diffraction patterns are in complete agreement with experimental observations and the mechanisms given in the literature. For AAS paste, however, the experimental observations and the obtained diffraction pattern are completely different compared to PC pastes. As seen, the XRD pattern of AAS paste showed no degradation products. The mechanism of deterioration due to sodium sulfate attack in AAS paste is, of course, different due to its different chemical and mineralogical phase compositions.

The appearance of calcite can be attributed to the hydration reactions of the slag. The formation of considerable amounts of calcium-silicate hydrate (CSH) is an indication of the presence of both amorphous calcium silicate and a few amounts of crystalline tricalcium silicate (as shown in Fig. 1) in the starting material. Hydration of these calcium silicates could result in the formation of calcium hydroxide in addition to CSH. This calcium hydroxide can be slowly carbonated to calcite by reacting with atmospheric carbon dioxide.

The absence of gypsum and ettringite in the structure of deteriorated AAS specimens can be attributed to the type of hydration products in AAS. The main hydration product formed during alkaline activation of the slag by using sodium silicate and sodium hydroxide is a poorly crystalline CSH, broadly similar to that formed in PCs, but with a lower Ca/Si ratio [27-29]. The CSH in the structure of AAS includes highly condensed anions with the contents of silicon in Q^2 and some in Q^3 sites. This favors the formation of cross-linked structures [30]. In these sites, the silicate ions are in dreierkette-type structure, i.e., chains of silicate tetrahedra formed by the alteration of pairs of tetrahedral directly bonded to a Ca-O layer and so-called bridging tetrahedral pointing away from this layer. Assuming, as is probable,

[Downloaded from sso.iust.ac.ir on 2025-12-10]

[DOI: 10.22068/ijmse.17.1.23]

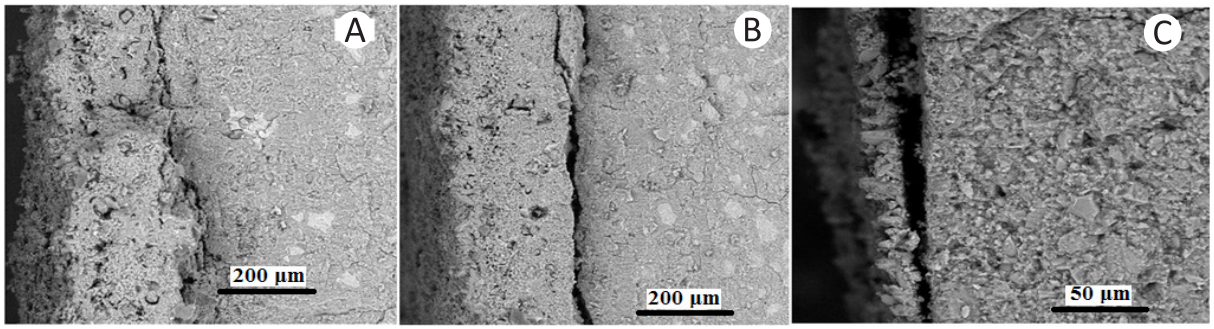

Fig. 10. SEM images (BSE mode) from cross sections of regions close to the exposed surfaces of the A) PC2, B) PC5, and C) AAS paste specimens.

that the chains are not terminated by bridging tetrahedron, the chain will be formed by (3n-1) tetrahedral [31-36]. Aluminum released during hydration of slag is distributed between CSH, aluminate hydrates, and any remaining unreacted slag. As mentioned, slag cements produce a CSH phase with a lower Ca/Si ratio, which allows it to bind more aluminum in its structure. Both CSH and aluminate hydrate can actually bind much of the aluminum and calcium ions released, hiding them from sulfate ions. Therefore, to a very large extent, the formation of gypsum and ettringite is prevented [37, 38]. In contrast, based on a mixed tobermorite-jennite model, Taylor [31] proposed a model for the CSH formed in PC pastes (Ca/Si=1.5), in which the absence of "bridging" sites produced the shortening of tetrahedral chains bound to Ca-O layers resulting in easier availability of calcium and aluminum for sulfate ions to form ettringite and gypsum.

3.5. Microstructural Studies

Fig. 10 shows BSE mode SEM images from cross-sections of regions close to the exposed surfaces of the PC2, PC5, and AAS paste specimens after 360 days of exposure.

As can be observed from Figs. 10A and 10B,

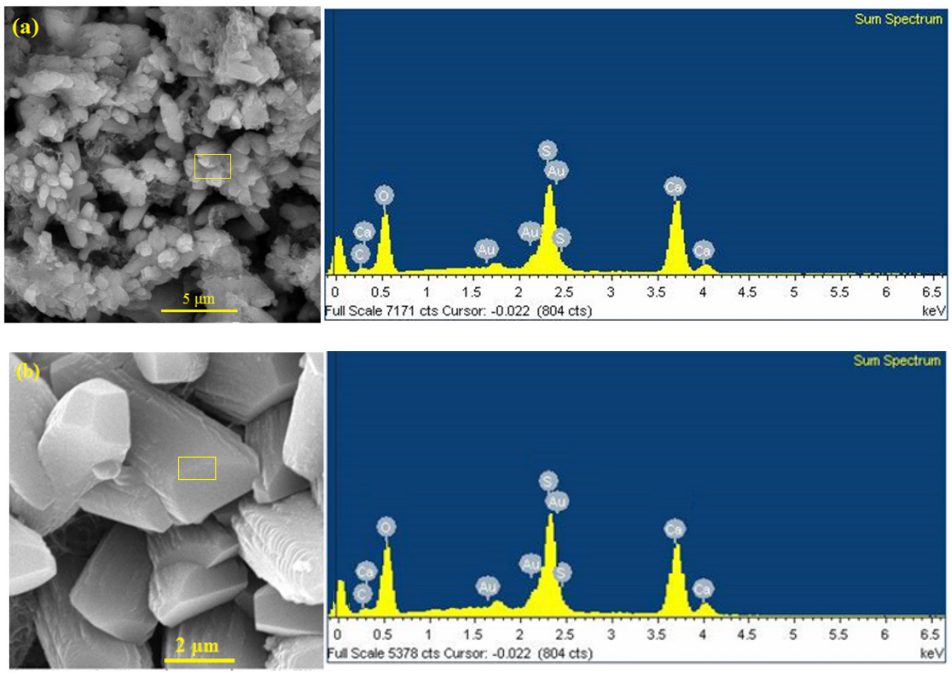

Fig. 11. SEM images of hexagonal rod-like gypsum crystals formed in the structure of a) PC2 and b) PC5 and respective EDAX analyses.

[Downloaded from sso.iust.ac.ir on 2025-12-10]

[DOI: 10.22068/ijmse.17.1.23]

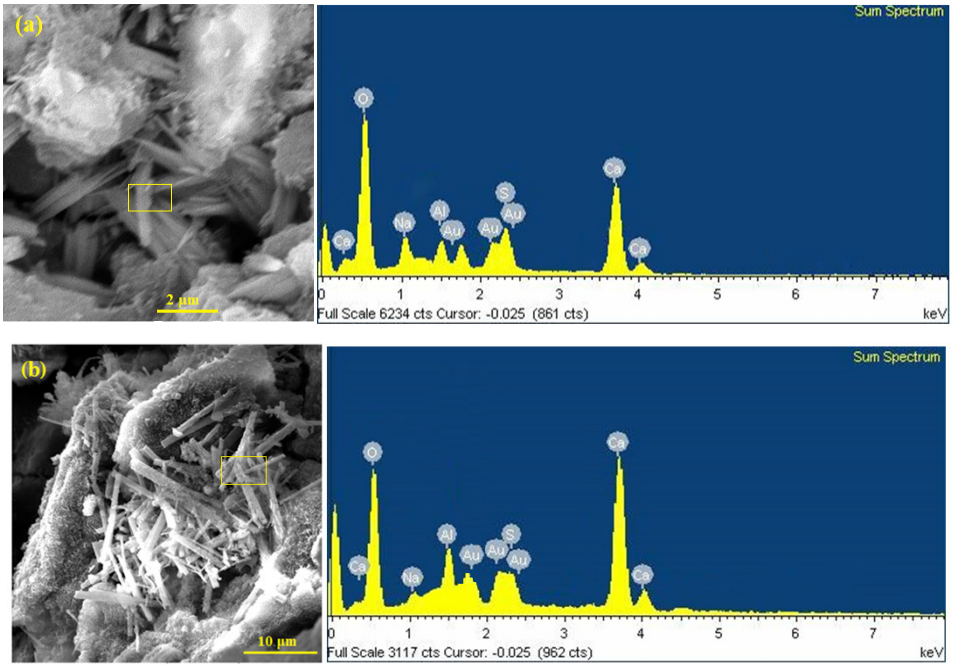

Fig. 12. SEM images of needle-like ettringite crystals formed in the structure of a) PC2 and b) PC5 and respective EDAX elemental analyses.

sulfate attack has caused a loose and porous surface layer in PC2 and PC5 paste specimens that is highly cracked. This is a soft surface layer that showed no or quite less adhesion and strength. In the case of AAS paste specimens (Fig. 10C), a detached surface layer can be seen.

The severity of deterioration which is due to crystallization of sodium sulfate and the occurrence of efflorescence phenomenon on the surface regions results in detachment of the surface parts from the paste specimens. SEM observations on paste specimens confirmed the extensive deposition of gypsum in the microstructure of PCs. Figs. 11a and 11b show hexagonal rod-like crystals of gypsum observed in PCs. The presence of gypsum crystals in the matrix has been confirmed by the results obtained from performing the elemental analyses using EDAX technique.

High calcium, oxygen, and sulfur peaks shown in the EDAX elemental spectra propose the presence of gypsum as the main phase in regions shown by rectangles in SEM micrographs. More accurate advanced studies by SEM led to the observation of needle-like ettringite crystals formed in the matrix of PC2 and PC5. Fig. 12 depicts SEM micrographs of ettringite crystals in PC2 and PC5 and respective EDAX elemental analyses. The EDAX analyses of regions specified by rectangles showed oxygen, sulfur, calcium, and aluminum in major quantities suggesting the presence of ettringite. As discussed by XRD patterns, the observation of ettringite crystals in the microstructure of PC2 and PC5 could be probable and expected due to the presence

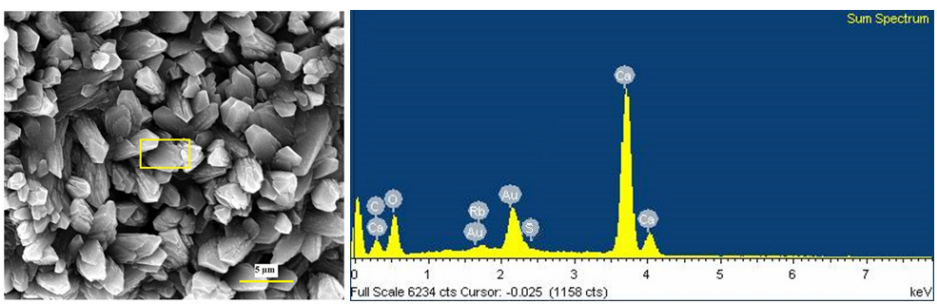

Fig. 13. SEM image and EDAX elemental analysis of hexagonal calcite crystals.

[Downloaded from sso.iust.ac.ir on 2025-12-10]

[DOI: 10.22068/ijmse.17.1.23]

of the C_3A phase in the composition of PCs. No ettringite and gypsum were discovered in the AAS matrix. These observations in the present study are in agreement with the findings of Bakharev et al. [4] in which AAS exposed to sodium sulfate solution showed no degradation products such as gypsum or ettringite.

As previously seen in XRD studies, calcite crystals were recognized by XRD analysis. The SEM micrograph of calcite crystals and also the confirmation of its presence in the AAS matrix by the EDAX elemental spectrum are shown in Fig. 13.

As seen, the elemental spectrum shows the presence of calcium, oxygen, and carbon as the main elements in the composition of the respective crystals. Calcite is formed on the surfaces of paste specimens exposed to a sodium sulfate solution. The presence of calcite is directly related to the calcium hydroxide existed in the matrix. The calcium hydroxide is converted into calcite over time as the result of contact with carbon dioxide existed in the air intensified due to exerting wetting-drying cycles. This finding is in agreement with findings presented by Veiga et al. [39] and Komljenovic et al. [40] which observed calcite crystals in AAS as a result of carbonation process during curing samples.

4. CONCLUSIONS

Sulfate resistance of alkali-activated slag (AAS) mortar in 5% sodium sulfate solution has been investigated and compared with types II and V Portland cements (PC2 and PC5). Prolonged exposure time resulted in the visual appearance of surface deterioration. Mortar specimens of PCs showed visually observable signs of expansion and cracking at the corners and regions close to the edges. In the case of AAS mortar, no visual sign of cracking was observed. The specimens instead showed some surface scaling. Compared to the compressive strengths measured at the beginning of the exposure time, after 360 days of exposure, PC2, PC5, and AAS cement have shown 71, 52 and 45% reduction in compressive strength, respectively. In addition, AAS mortar specimens exhibited the least changes in length in comparison with PC2 and PC5. No ettringite and gypsum was found in the hardened paste of AAS confirmed by XRD and SEM/EDAX studies. According to the observations and obtained results, under the tested conditions, AAS cement exhibited a higher sodium sulfate resistance than PC2 and PC5.

REFERENCES

1. Puertas, F., Palacios, M., Gil-Maroto, A. and Vázquez, T., "Alkali-aggregate behaviour of alkali-activated slag mortars: Effect of aggregate type". Cem. Concr. Compos., 2009, 31, 277–284.
2. Jiang, M., Chen, X., Rajabipour, F., Asce, A. M., Hendrickson, C. T. and Asce, D. M., "Comparative life cycle assessment of conventional, glass powder and alkali-activated slag concrete and mortar". J. Infrastruct. Syst., 2014, 20, 0401-4020.
3. Puertas, F., Martinez-Ramirez, S., Alonso, S. and Vasquez, T., "Alkali activated fly ash/slag cement and Strength behavior and hydration products". Cem. Concr. Res., 2000, 30, 1625–1632.
4. Bakharev, T., Sanjayan, J. G. and Cheng, Y. B., "Sulfate attack on alkali-activated slag concrete. Cem". Concr. Res., 2002, 32, 211-216.
5. Bakharev, T., Sanjayan, J. G. and Cheng, Y. B., "Resistance of alkali activated slag concrete to acid attack". Cem. Concr. Res., 2003, 33, 1607-1611.
6. Talero, R., "Sulfate resistant Portland cements are not the ultimate answer to the problem of sulfate attack". International congress. Quim. Cim. [An.], 1986, 5, 151– 158.
7. Lawrence, C. D., "Sulfate attack on concrete". Mag. Concr. Res., 1990, 42, 249–264.
8. Al-Amoudi, O. S. B., "Performance of fifteen reinforced concretes in magnesium–sodium sulfate environments". Constr. Build. Mater., 1995, 9, 25–33.
9. Al-Amoudi, O. S. B., Maslehuddin, M. and Saadi, M. M., "Effect of magnesium sulfate and sodium sulfate on the durability performance of plain and blended cements". ACI Mater. J., 1995, 92, 15–24.
10. Mehta, P. K., "Sulfate attack on concrete". Univ. Autonoma de Nuevo Leon, 1993, 107– 132.
11. Taylor, H. F. W., "Cement Chemistry", 2nd

[Downloaded from sso.iust.ac.ir on 2025-12-10]

[DOI: 10.22068/ijmse.17.1.23]

Edition, Thomas Telford publishing Ltd. Services, London, Great Britain, 1997.
12. Felekoglu, B., Ramyar, K., Tosun, K. and Musal, B., "Sulfate resistances of different types of Turkish Portland cements by selecting the appropriate test methods. Constr". Build. Mater., 2006, 20, 819-823.
13. Schmidt, T., Lothenbach, B., Romer, M., Neuenschwander, J. and Scrivener, K., "Physical and microstructural aspects of sulfate attack on ordinary and limestone blended Portland cements". Cem. Concr. Res., 2009, 39, 1111-1121.
14. Atahan, H. N. and Dikme, D., "Use of mineral admixtures for enhanced resistance against sulfate attack. Constr". Build. Mater., 2011, 25, 3450–3457.
15. Harald, J., "Thaumasite formed by sulfate attack on mortar with limestone filler". Cem. Concr. Compos., 2003, 25, 955–959.
16. Thorvaldson, T., Wolochow, D. and Vigfusson, V. A., "Studies of the action of sulfates on Portland cement". Can. J. Res., 1932, 6, 487–517.
17. Miller, E. W., "Blended Cements, Applications and implications". Cem. Concr. Compos., 1993, 15, 237-245.
18. Fu, X., Hou, W., Yang, C., Li, D. and Wu, X., "Studies on Portland cement with large amount of slag". Cem. Concr. Res., 2000, 30, 645-649.
19. Wu, Z. and Naik, T. R., "Properties of concrete produced from multicomponent blended cements. Cem". Concr. Res., 2002, 32, 1937-1942.
20. Allahverdi, A., Akhondi, M. and Mahinroosta, M., "Superior sodium sulfate resistance of a chemically activated phosphorus slag–based composite cement". J. Mater. Civil Eng., 2017, 29, 1-9.
21. Leonard, S. and Bentur, A., "Improvement of the durability of glass fiber reinforced cement using blended cement matrix". Cem. Concr. Res., 1984, 14, 717-728.
22. Teoreanu, I., Volceanov, A. and Stoleriu, S., "Non Portland cements and derived materials". Cem. Concr. Compos., 2005, 27, 650-660.
23. Zhao, F. Q., Ni, W., Wang, H. J. and Liu, H. J., "Activated fly ash/slag blended cement". Resour. Conserv. Recycl., 2007, 52, 303-313.
24. Bin, X. and Xincheng, P., "Study on durability of solid alkaline AAS cement", Proceeding of second International Conference on Alkaline cement and concrete, Kyiev, Ukraine, 1999.
25. ASTM, Standard test method for length change of hydraulic cement mortars exposed to a sulfate solution, ASTM C1012, West Conshohocken, PA, 2015.
26. Gong, K. and White, C. E., "Nanoscale chemical degradation mechanisms of sulfate attack in alkali-activated slag". J. Phys. Chem. C, 2018, 122, 5992–6004.
27. Puertas, F., "Cementos de Escorias Activadas Alcalinamente: Situacion Actual Qqy Perspectivas de Futuro". Materiales de Construcción (Spain), 1995, 45, 53-64.
28. Wang, S. D. and Scrivener, K. L., "Hydration products of alkali activated slag cement". Cem. Concr. Res., 1995, 25, 561-571.
29. Fernandez-Jimenez, A., "Cementos de Escorias Activadas Alcalinamente: Influencia de las Variables y Modelizacion del Proceso". Thesis, Universidad Autonoma de Madrid (U.A.M), Spain, 2000.
30. Fernandez-Jimenez, A. and Puertas, F., "Structure of Calcium Silicate Hydrates Formed in Alkaline-Activated Slag: Influence of the Type of Alkaline Activator". J. Am. Ceram. Soc., 2003, 86, 1389-1394.
31. Taylor, H. F. W., "Proposed Structure for Calcium Silicate Hydrate Gel". J. Am. Ceram. Soc., 1986, 69, 464–67.
32. Richardson, I. G. and Groves, G. W., "The Incorporation of Minor and Trace Elements into Calcium Silicate Hydrate (C-S-H) Gel in Hardened Cement Pastes". Cem. Concr. Res., 1993, 23, 131-138.
33. Richardson, I. G., Brough, A. R., Groves, G. W. and Dobson, C. M., "The Characterisation of Hardened Alkali-Activated Blast-Furnace Slag Pastes and the Nature of the Calcium Silicate Hydrate (C-S-H)". Cem. Concr. Res., 1994, 5, 813-829.
34. Schilling, P. J., Butler, L. G., Roy, A. and Eaton, H. C., " ^{29}Si and ^{27}Al MAS-NMR of NaOH Activated Blast-Furnace Slag". J. Am. Ceram. Soc., 1994, 77, 2363-2368.
35. Richardson, I. G., "The Nature of C-S-H in Hardened Cements". Cem. Concr. Res., 1999, 29, 1131-1147.
36. Richardson, I. G. and Cabrera, J. G., "The Nature of C-S-H in Model Slag Cements". Cem. Concr. Compos., 2000, 22, 259-266.
37. Gollop, R. S. and Taylor, H. F., "Microstructural

[Downloaded from sso.iust.ac.ir on 2025-12-10]

[DOI: 10.22068/ijmse.17.1.23]

and microanalytical studies of sulfate attack", V, comparison of different slag blends. Cem. Concr. Res., 1996, 27, 1029–1044.
38. Gollop, R. S. and Taylor, H. F., "Microstructural and microanalytical studies of sulfate attack IV – reactions of a slag cement paste with sodium and magnesium sulfate solutions". Cem. Concr. Res., 1996, 26, 1013–1028.
39. Veiga, K. K. and Gastaldini, A. L. G., "Sulfate attack on a white Portland cement with activated slag". Constr. Build. Mater., 2012, 34, 494–503.
40. Komljenovic, M., Bašcarevic, Z., Marjanovic, N. and Nikolic, V., "External sulfate attack on alkali-activated slag". Constr. Build. Mater., 2013, 49, 31–39.

[Downloaded from sso.iust.ac.ir on 2025-12-10]

[DOI: 10.22068/ijmse.17.1.23]